




Eckhaus selection: The mechanism of pattern persistence in a reaction-diffusion systemAldo Ledesma-Durán ^{*}, E. A. Ortiz-Durán , and J. L. Aragón*Centro de Física Aplicada y Tecnología Avanzada, Universidad Nacional Autónoma de México, Boulevard Juriquilla 3001, Juriquilla, 76230 Querétaro, Mexico*Iván Santamaría-Holek *Unidad Multidisciplinaria de Docencia e Investigación, Facultad de Ciencias, Universidad Nacional Autónoma de México, Boulevard Juriquilla 3001, Juriquilla, 76230 Querétaro, Mexico*

(Received 14 June 2020; accepted 1 September 2020; published 15 September 2020)

In this work, we show theoretically and numerically that a one-dimensional reaction-diffusion system, near the Turing bifurcation, produces different number of stripes when, in addition to random noise, the Fourier mode of a prepattern used to initialize the system changes. We also show that the Fourier modes that persist are inside the Eckhaus stability regions, while those outside this region follow a wave number selection process not predicted by the linear analysis. To test our results, we use the Brusselator reaction-diffusion system obtaining an excellent agreement between the weakly nonlinear predictions of the real Ginzburg-Landau equations and the numerical solutions near the bifurcation. Although the persistence of patterns is not relevant as a simple generating mechanism of self-organization, it is crucial to understand the formation of patterns that occurs in multiple stages. In this work, we discuss the relevance of our results on the robustness and diversity of solutions in multiple-steps mechanisms of biological pattern formation and auto-organization in growing domains.

DOI: [10.1103/PhysRevE.102.032214](https://doi.org/10.1103/PhysRevE.102.032214)**I. INTRODUCTION**

Reaction-diffusion (RD) equations provide a standard model for many biological, chemical, and social dynamical systems since, near the Turing bifurcation, an essential ingredient in modeling auto-organization processes takes place: the emergence of steady spatial patterns.

A key feature of this process is determined by the initial conditions, which provide the available Fourier modes of the RD equations that grow or decay according to the dynamics. Since the RD equations usually involve nonlinear terms, tracking the dynamics of each mode for predicting the steady solution is a difficult task. Most of the models using RD equations are initialized with a small random spatial perturbation around the equilibrium concentrations. In this case, the steady spatial pattern is given by the fastest growing mode predicted by the linear analysis. This constitutes the approach for models of spatial pattern formation where it is thought that *all* initial non zero Fourier modes are, in principle, equally probable when the spatial auto-organization is mainly initiated by the inherent spatial fluctuations and not by a prior configuration or prepattern.

In their pioneering work on the sensitivity to initial conditions on Turing patterns, Arcuri and Murray [1] showed that random initial conditions around the equilibrium points lead the emerging pattern to the expected wave number in a robust way. This is the faster growing wave number of the dispersion relation obtained from the linear analysis. But they also noticed that if the steady spatial pattern solution of a RD

mechanism with different dynamics (and consequently with a different final wave number) is used as initial condition or prepattern, some initial configurations can *persist*. We say that a pattern persists when the steady pattern has the same wave number that the initial pattern.

In this work we study RD systems where, in addition to the *small* random noise due to fluctuations, there is a preponderant Fourier mode in the initial conditions. To focus on the role of these initial conditions, we show that the possible stable configurations (i.e., those that can persist) are obtained by fixing factors, such as the parameter values, domain size, and boundary conditions. We show that this persistence occurs in systems near the Turing bifurcation provided that the wave number of the prepattern is inside the Eckhaus region. Initial spatial configurations with wave numbers outside this region break into a spatial pattern with stable wave number by forming dislocations or defects.

Here the Brusselator RD system is used, in particular we study its amplitude Ginzburg-Landau (GL) equation, which predicts the evolution of the envelope, the number of stable configurations and the free energy of the systems in a weakly nonlinear approach [2]. Our predictions are corroborated by numerical solutions of the one-dimensional Brusselator. Within the same approach it will be also studied how the amplitude and wave number of the spatial configuration, as function of time, are related with changes in the free energy of the system thus allowing to understand the stability and robustness of the solutions on a thermodynamical basis.

An exciting application of these results to biology is related with the fact that a multistep mechanism of spatial organization occurs in subsequent stages. When the last stage is of RD kind, with a different wave number than the predicted by

*Corresponding author: aldo_ledesma@ciencias.unam.mx

the linear analysis, then the pattern persistence mechanism that we discuss in this work is of high relevance. Examples of multistep mechanisms of pattern formation are ubiquitous in developmental Biology [3]. The most important example occurs in morphogenesis where the formation of structures obtained by a RD mechanism depends on the properties and geometries of previous ones. Also in a growth process where the pattern which corresponds to an organized physiological structure at a specific time does not start randomly at each stage but depends on the spatial pattern achieved at some previous time. These biological implications are also discussed and exemplified.

II. THEORETICAL ANALYSIS

The one-dimensional RD Brusselator system is given by

$$\frac{\partial u}{\partial t} = \sigma \frac{\partial^2 u}{\partial x^2} + A - (B + 1)u + u^2 v, \quad (1)$$

$$\frac{\partial v}{\partial t} = \frac{\partial^2 u}{\partial x^2} + Bu - u^2 v, \quad (2)$$

where $\mathbf{u} = (u, v)$ are the two chemical concentrations. In this work we keep $A = 1$, $\sigma = 0.1$, and the domain size $L = 15 \cdot (2\pi/k_c)$ fixed and periodic boundary conditions are assumed. If B is used as bifurcation parameter, the Turing bifurcation arises for solutions with critical wave number $k_c = \sqrt{A/\sqrt{\sigma}}$ and $B \leq B_T \equiv (1 + A\sqrt{\sigma})^2$, where B_T is the bifurcation value. The chosen domain size guarantees that there are exactly $n_c = 15$ stripes at the bifurcation. The expected wave number is that of maximum growth in the linear dispersion relation and is given by

$$k_l^2 = \frac{A\sqrt{B\sigma} + \sigma(1 - A^2 - B + A\sqrt{B\sigma})}{(1 - \sigma)\sigma}, \quad (3)$$

which predicts that the expected wave number increases as B increases.

A system with initial conditions given by $\mathbf{u}(x, t = 0) = \mathbf{u}_0 + \xi(x)$ is expected to produce a pattern with wave number k_l , where $\mathbf{u}_0 = (A, B/A)$ are the equilibrium concentrations and $\xi(x)$ is white noise with a small amplitude compared with $|\mathbf{u}_0|$. This essentially summarizes the linear analysis.

Near the bifurcation, a weakly nonlinear study can be applied to obtain perturbative approximate solutions of the Brusselator [4]. These solutions are proportional to the distance to the bifurcation $\epsilon^2 = (B - B_T)/B_T$ and their dynamics obey a real GL equation. This means that if we assume an approximate solution of the RD of the form $\mathbf{u} \approx \mathbf{u}_0 + T(x, t)e^{ik_c x} \mathbf{e}_T + \text{c.c.}$, with \mathbf{e}_T the linear eigenvector, the amplitude $T(x, t)$ fulfills:

$$\frac{\partial T}{\partial t} = \mu_t T - a_t |T|^2 T + b_t \frac{\partial^2 T}{\partial x^2}, \quad (4)$$

The GL approach to pattern formation has been widely used and the main results related to persistency of patterns are summarized here; for a more detailed account see for instance Refs. [5,6]. The coefficients in Eq. (4) are given, for instance in Refs. [7,8]. For the assumed values of A and σ , these coefficients are $\mu_t = 0.8441(B - B_T)$, $a_t = 1.664$ and $b_t = 0.3376$.

Equation (4) has a family of Turing solutions consisting of steady patterns $T(x, t) = T(x) = T_s e^{iQx}$, where $T_s = \sqrt{(\mu_t - b_t Q^2)/a_t}$ is a constant that corresponds to the amplitude of the main wave mode (excluding the zero mode), and Q measures the deviation of the wave number respect to the critical value k_c , that is $Q = k - k_c$. The solution exists provided that the term in the square root of T_s is positive.

The solutions of the RD system initialized with

$$\mathbf{u}(x, t = 0) = \mathbf{u}_0 + [T_s e^{i(k_c + Q)x} \mathbf{e}_T + \text{c.c.}] + \xi(x), \quad (5)$$

are Eckhaus stable (preserve their wave number) as long as the Eckhaus criterion is fulfilled [9,10]:

$$Q^2 < Q_{\text{Eck}}^2 = \left(\frac{1}{3}\right) \frac{\mu_t}{b_t}. \quad (6)$$

Otherwise, the solution is Eckhaus unstable and the spatial pattern initialized with wave number $k = k_c + Q$ changes its initial wave number, producing defects/dislocations in the horizontal alignment of the stripes as viewed in the space-time map solutions of the one-dimensional RD system [11].

The time evolution of the amplitude $T(x, t)$ in Eq. (4) has the gradient form $\partial T/\partial t = -\delta\mathcal{V}/\delta T$ with the potential functional given by

$$\mathcal{V}(t) = \frac{1}{2} \int_0^L dx \left\{ -\mu_t |T|^2 + \frac{a_t}{2} |T|^4 + b_t \left| \frac{\partial T}{\partial x} \right|^2 \right\}. \quad (7)$$

The GL equation of motion then implies that

$$\partial\mathcal{V}/\partial t = - \int_0^L |\partial T/\partial t|^2 dx, \quad (8)$$

hence the value of \mathcal{V} decreases and, since it is bounded from below, it plays the role of a Lyapunov functional or generalized free energy [12,13]. This means that the evolution of the system tends to minimize the free energy of the system [5,6]. It should be stressed that Eq. (7) is a Lyapunov functional for the amplitude T satisfying the GL Eq. (4). Therefore, the stability of the equilibrium point u_0 of the RD system Eqs. (1) and (2), as deduced from this Lyapunov functional, is only valid near the bifurcation where the GL approach provides a good approximation of the solution [14,15].

Equation (7) is difficult to corroborate numerically. However, a form of the energy can be obtained by considering that all the solutions of Eq. (4) can be written as $T = R(x, t)e^{i\theta(x, t)}$, being R and θ the modulus and the phase of the amplitude T , respectively. By substituting this expression in Eq. (4), differential equations for R and θ are obtained. From the equation for θ we get that the stationary solutions satisfy $J = R^2 \partial\theta/\partial x = \text{const.}$, and from the equation for R it follows that the modulus obeys an equation analogous to Newton's equation of motion for a particle in a potential $U(R) = 1/2(\mu_t R^2 - a_t R^4/2 + b_t J^2/R^2)$ [16]. By taking into account the stationary solutions, a comparison with $T = T_s e^{iQx}$ yields $R = T_s$ and $J = T_s^2 Q$. Substituting the value of T_s as function of Q allows us to obtain a quartic potential for the wave number deviation as

$$U(Q) = \frac{3b_t^2}{4a_t} (Q^2 + Q_{\text{Eck}}^2)(3Q_{\text{Eck}}^2 - Q^2). \quad (9)$$

This kind of potential energy has a minimum in $Q = 0$ and two maxima in $Q = \pm Q_{\text{Eck}}$, thus the Eckhaus instability

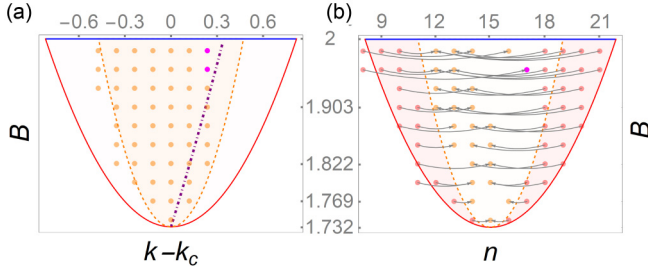


FIG. 1. Stable (orange-shaded zone) and unstable modes (pink-shaded zone) of the Brusselator, characterized by the bifurcation parameter B , (a) as a function of the distance $Q = k - k_c$ to the bifurcation and the wave number of the initial condition, and (b) as a function of the number of rolls at the beginning of the process, n . The existence curve (orange-dashed line) is obtained from the condition $T_s > 0$, whereas the instability curve (red solid line) from Eq. (6). The transition from unstable to stable zone is indicated by curved arrows in panel (b).

Eq. (6) is confirmed from an energetic point of view. This means that the prepatterns with wave numbers k such that $|k - k_c| < Q_{\text{Eck}}$ can persist under the dynamics of the RD system, at least near the bifurcation. The available wave number must also satisfy the finite-length boundary condition, $k = 2n\pi/L$, with n an integer, consequently the persistence or transition among states occurs in discrete steps.

In the next Section these predictions are numerically validated. Therefore, it will be verified that the RD system can produce different patterns under changes of the initial conditions. The amplitudes of the Fourier modes of the solution, as function of time, will be measured and we will try to link these amplitude values with the free energy of the steady pattern and the role of noise on the persistence of patterns.

III. NUMERICAL RESULTS

In this section the Brusselator system Eqs. (1) and (2) will be numerically solved using the finite element software COMSOL Multiphysics, with an adaptative one dimensional mesh initialized with 100 evenly spaced nodes, with periodic boundary conditions, and a time step which provides 10 000 steps of recurrence. The total time $t_{\text{max}} = 100/\mu_t$ used for the simulations depends on the distance to the bifurcation and is based on the characteristic time of each process.

In Fig. 1 the stable and unstable solutions of the Brusselator are plotted. The existence curve (orange dashed line) is obtained from the condition $T_s > 0$ and the instability curve (red solid line) from (6), in terms of the bifurcation parameter B and the wave number deviation, $Q = k - k_c$ (left), or the number of rolls at the beginning of the process, n (right). The blue line is the boundary with the Hopf bifurcation, $B_H = 1 + A^2 = 2$. Therefore, the orange and red regions represent the initial configurations in Eq. (5) where the theoretical formalism predicts stable and unstable solutions, respectively.

In Fig. 1(a), orange points represent the numerical solutions that remain stable. Magenta points represent Mixed mode solutions, which occurs due to the proximity to the Hopf bifurcation. In Fig. 1(b) the unstable numerical solutions are plotted. The red points represent the initial wave number and

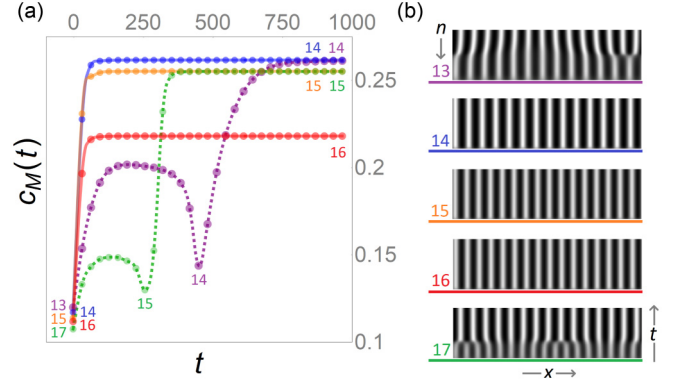


FIG. 2. Evolution of the system initialized with a different number of rolls. (a) The amplitude of the main Fourier coefficient c_M versus time; each solution was initialized with initial Fourier mode n (colored numbers), with $B = 1.769$. The joined curves indicate the time evolution of each mode until it reaches a stationary state. Some initial modes (17 and 13) reach stationarity after passing through an intermediate Fourier mode. These features are illustrated in the time-space maps displayed in panel (b).

the orange points, the final wave number of the numerical pattern. The transition in each case is represented by an arrow. As it can be seen, the comparison between theoretical and numerical results is satisfactory, mainly for values of B near the bifurcation. It is also observable the asymmetry towards negative values of Q of the orange dots in Fig. 1. It is important to remark that this tendency toward patterns with less rolls, as B increases, observed in Fig. 1(b) does not correspond to the predictions of the linear analysis, depicted as a purple line in Fig. 1(a), where the most rapid growing mode k_l in Eq. (3) is plotted.

These results show that, as predicted by the amplitude formalism, the central zone of Fig. 1 (near $k = k_c$) is occupied by stable pattern solutions, which preserve the information of the prepattern. In contrast, when the solutions were initialized with wave numbers outside this region, the system tends to change its spatial configuration to solutions with wave numbers in the stable region. We conclude that there is a limited range of different possible outputs (steady patterns with different number of stripes) that increases quadratically with the distance to the bifurcation.

In Fig. 2 we plot the value of the main Fourier coefficient c_M of each solution initialized with initial Fourier mode n as a function of time, for $B = 1.769$. In Fig. 2(a), the curves that correspond to stable solutions (solid lines) grow monotonically up to their asymptotic value for the corresponding Fourier mode. In contrast, for unstable initial conditions (dashed lines), the initial Fourier mode loses amplitude until a new mode enters, with an amplitude that grows up to its final value. This can be followed in the spatiotemporal maps of the solutions plotted in Fig. 2(b), where changes in the amplitude of the initially stable solutions, as well as changes due to dislocations and defects of the unstable solutions, are illustrated by means of the contrast in the gray scale.

The transition from instability to stability can occur in multiple stages as illustrated in Fig. 3(a), where several transitions are tracked. The initial Fourier mode of the solution is

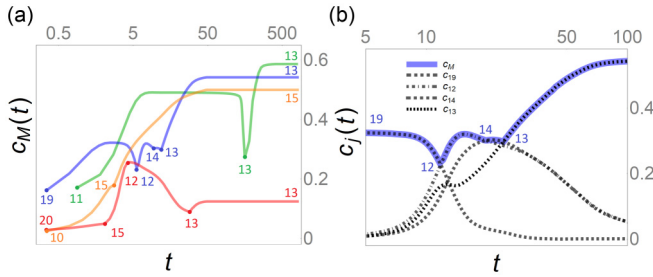


FIG. 3. Temporal evolution of the main Fourier coefficient c_M for systems initialized in the unstable region [pink zone in Fig. 1(b)]. (a) The colored numbers indicate the number of initial rolls. The lines show that multiple transitions may occur before reaching the preponderant stationary mode. (b) An illustration of the fate of the unstable modes and the transition mechanism towards mode stability. See the main text for more details.

indicated at the beginning of each curve; each Fourier spectrum can be followed and during the evolution some others Fourier modes appear and dominate until stability is reached. For example, the mode with 19 rolls, as time goes shows an initial increasing of its amplitude, followed by a decrease until the mode with 12 rolls enters; this mode also grows its amplitude which again decreases just before the mode with 14 rolls appears; finally, the 13 rolls mode dominates, which grows until stability is reached. The multiple transition occurs more frequently for values of B far from the bifurcation, as it occurs in Fig. 3(a), where $B = 1.903$. Notice that in several cases the transition among different patterns occurs through a slow decrease in the amplitude of the outgoing mode followed by a rapid outburst of the new mode. The process for each Fourier mode is exemplified in Fig. 3(b), where the observable wave number of the pattern corresponding to c_M (plotted in blue) is decomposed in the amplitudes of the different modes c_j (black lines) entering in the solution.

To relate the persistence of patterns with the energy of the system and the initial conditions in the stable region, and their rearrangements, when they are in the unstable region, in Fig. 4(a) the amplitude of the steady pattern $c_M(t \rightarrow \infty)$ for different initial configurations is measured. This is done for three different values of B , namely, 1.769 (circles), 1.822

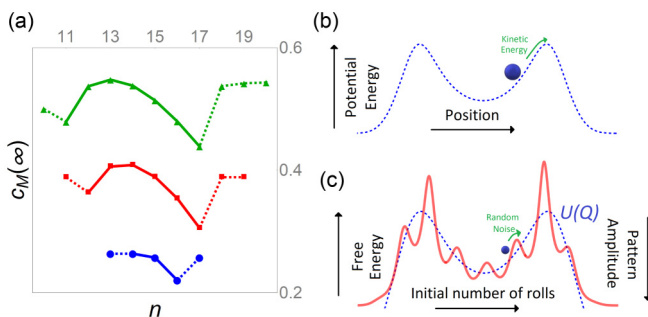


FIG. 4. Relation between the amplitude of the observable pattern and the energy of the system. (a) Amplitude of the maximum Fourier coefficient in the steady state as a function of the number of rolls in the initial condition. (b, c) Analogy of the persistence and unstabilization of pattern in terms of the energy landscape of the system.

(squares), and 1.903 (triangles). As it can be seen, the persistent prepatterns (joined by solid lines) have a kind of parabolic profile. Near the unstabilization, the amplitude reaches a local minimum from where the adjacent unstable prepatterns (joined by dashed lines) increase their amplitude. This reminds the energy profile described by Eq. (9) and plotted as a blue line in Fig. 4(c). The energy profile $U(Q)$ establishes that prepatterns in the stable region are localized inside a basin of energy with minimum value at $k = k_c$; outside this basin ($|Q| \geq Q_{Eck}$), prepatterns should rearrange to decrease the energy of the system.

This analogy between the amplitudes of the steady pattern and the initial energy of the dynamical system, together with the minimization of the functional Eq. (9), suggests that the persistence of multiple patterns and the unstabilization of others can be understood as marbles rolling in a bowl, as described in Fig. 4(b). A marble thrown near the base (initial conditions with n_c stripes) will remain in the base of the bowl (the critical number of stripes). If the marble is placed in the bowl with an adequate initial energy (initial conditions with n in the stable region), the marble can continue rolling with a certain height inside the bowl (a number of stripes different to n_c). The final height of the marble (the final number of stripes) depends on the balance between the initial position (potential energy) and the initial kinetic energy; in the case of the prepatterns, the amplitude and wave number of the steady pattern depends on the amount of energy necessary to form the initial prepattern (free energy), as illustrated in Fig. 4(c). In this case, the intensity of the initial random noise can act as thermal energy at the beginning of the process, which can take the system from one local minimum to another (i.e., from a given number of stripes to another). In the case studied here, the spatial fluctuations appear just at the beginning of the process, however, in RD systems with additive noise, the random contribution occurs during the entire process and plays the role of a thermal bath [17–19]. The magnitude of those fluctuations coupled with the energy landscape determine the wave number of the steady solution. This energy landscape schematically sketched in the red curve of Fig. 4(c) results from Eq. (9) and the fact that patterns in RD system have only an integer number of lines.

The destabilizing role of the initial noise as a function of the initial number of stripes is depicted in Fig. 5. The amplitude of the initial spatial noise, as a function of the initial number of stripes, is measured as the maximum value of $|\xi(x)|$. Each color line corresponds to the noise intensity, where each Eckhaus stable mode loses stability. The values of B coincide with those of Fig. 4 and the same color code is used. Clearly, for B values far from the bifurcation (green case), the magnitude of the noise unstabilizing the solution is broader and tends to the left side, in contrast to closer values (blue case). Symbols represent the numerical solutions where the initial preponderant mode persists in the range studied, showing a similar distribution as the one of the continuous line.

IV. BIOLOGICAL IMPLICATIONS

In the previous section we shown that a RD system with the same set of parameters (in the case of the Brusselator, A,

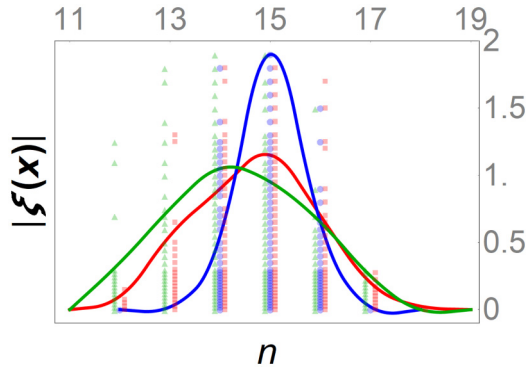


FIG. 5. Intensity of the noise that unstabilize a pattern initiated with n stripes. Color values are the same as in Fig. 4(a). Lines indicate the first occasion that the pattern loses stability and symbols reflected the cases when the initial solution persists in our numerical exploration of the region.

B , and σ) and fixed domain size (L) can produce multiple steady pattern solutions depending on the initial conditions. As long as a *single mechanism* of pattern formation is considered, these predictions seem to have not many applications since, to set up the different stable spatial configurations, the multiplicity should be established from the very beginning. However, a *multiple-steps mechanism* of pattern generation can produce solutions with: (1) a variety of spatial patterns and (2) a limited number of possible solutions. This may be an attractive idea for the problem of biological variation, where the variation of traits related to phenotypic characters (coat color, teeth number, feather buds, hair follicles, etc.) in individuals of the same specie or genus (or even in the same individual in different stages of its development) are related to multiple mechanisms of phenotypic trait differentiation (as genetic differences, epigenetic factors and phenotypic plasticity) [20,21].

The Turing mechanism of pattern formation has the advantage of producing a steady spatial pattern from practically homogeneously distributed systems [22]. The effective wave number can be determined from the linear analysis as the most rapid growing mode k_l and, in a finite one dimensional domain, the pattern has always $n \approx k_l L / (2\pi)$ stripes [23]. Therefore, in the context of *one-stage* mechanism of Turing pattern formation, the trait variation of some feature labeled by n has at least four possible candidates: (1) variation of physicochemical parameters; (2) variation of the domain length; (3) variation in the initial intensity and randomness of the initial conditions; and (4) different boundary conditions and domain shapes [24]. If a Turing solution in our models is interpreted as the average trait exhibited by different individuals, then the phenotypic variations can be understood as random substitutions in some of these factors.

From our results, the possibility of a less obvious mechanism arises, where the phenotypic variability of traits are not only attributed to perturbations of the physicochemical aspects of a Turing RD mechanism, which gives place to the spatial organization of morphogens, but to the sequence of previous stages during the development process [25–28].

In a *two-stages* mechanism of pattern organization, for example, there could be a finite number of possible previous prepatterns generated by a nonrobust mechanism of pattern formation, and then, in a second stage, the information of the first prepattern is encoded into a initial genetic expression which determines how the morphogens are initially distributed as input for the second stage, where a RD mechanism can preserve the spatial stable pattern or lead unstable configurations to stable ones. In this way, the first nonrobust mechanism produces multiple and variable patterns and the second one takes this information to produce a limited variability.

For illustrative purposes only, let us consider these two oversimplified development models related with the variation in the number of stripes in the skin of some individuals of the same species.

In the first model, illustrated in Fig. 6(a), a single-stage mechanism of pattern formation is considered, where perturbations at the genetic/epigenetic level produce a disperse distribution of the already mentioned factor(s) in the RD system among different individuals. Let us denote this random factor generically as β . The variation of this parameter in turn produces different number of skin stripes, labeled by n . Therefore, the distribution of individuals with a certain number of stripes $s(n)$ can be deduced from the distribution curve of β , $r(\beta)$ as depicted in Fig. 6(a).

In the second model, illustrated in Fig. 6(b), a two-stages mechanism of pattern formation is considered. The first organization mechanism produces several spatial configurations among different individuals. These prepatterns p will be the initial array of morphogens of the second RD mechanism that will produce skin stripes. The first stage can be a RD mechanism [29,30], a positional information (PI) gradient [31,32], heterochrony (HC) [33,34], or any mechanism of spatial pattern formation that produces a wide variety of prepatterns distributed according to a certain distribution $r(p)$. The information of these prepatterns is encoded and serves as input of the second stage in the development process, where a RD mechanism can either preserve the spatial information of the stable configurations (those with an *adequate* number of stripes) or can stabilize unstable configurations (those resulting in too many or too few stripes). The range of the adequate number of stripes is now directly dictated by physicochemical parameters and the size of the skin and, in this way, even in the case when these factors are practically the same among many individuals, there is a *restricted variability* in the phenotypic trait due to the interaction of the two stages of the process. This can be identified as a distribution $s(n)$ with very short tails.

It could also be possible that the variability of some trait in different individuals is due to a combination of characters of both of models [35–37], but it is clear that a phenotypic trait does not occur as an isolated process but it is usually the result of a temporal succession of multiple stages [38–41]. The same applies for the process of growing where the exhibited pattern depends not just in the current domain sizes domain at time t , but also in terms of the stability of the prepattern at time $t - \Delta t$. Persistence of patterns results a fundamental issue to include in processes where time plays a role [42–45].

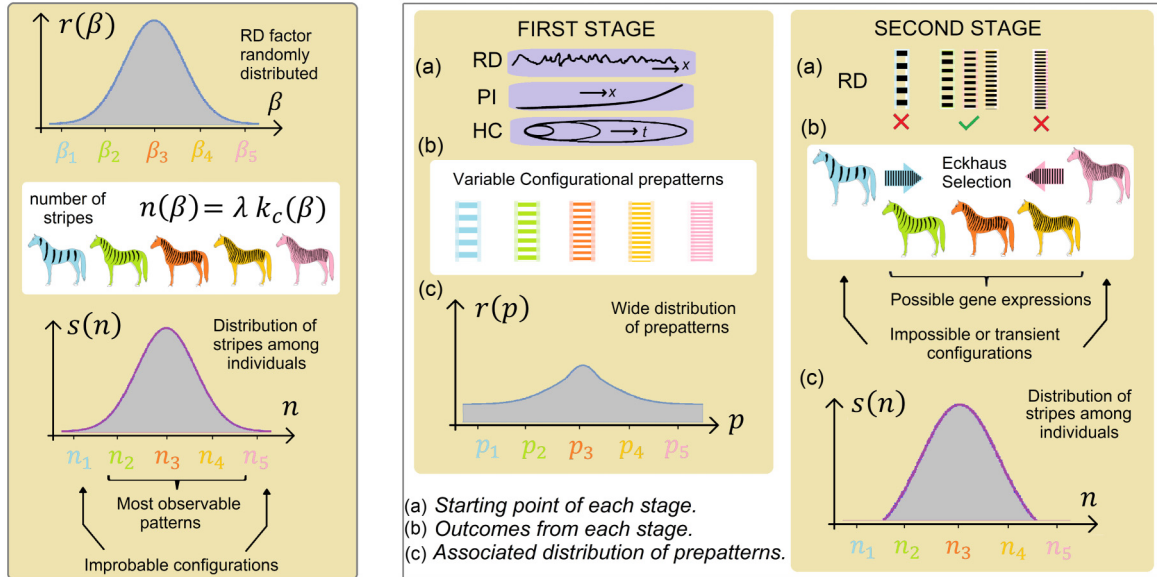


FIG. 6. Two models to understanding biological variation of phenotypic trait formed by a RD mechanism, like the number of skin stripes. One-stage process (left) or multiple stages process (right).

V. DISCUSSION AND CONCLUSIONS

In this work we shown that a RD system initialized with a preponderant Fourier mode underlying the random spatial initial conditions tends to preserve the spatial configuration when it is near the bifurcation values. To show this, the amplitude formalism near the Turing bifurcations was applied, which turned out to be successful for predicting how many stable rolls can contain a system in terms of the Eckhaus instability. Our results contribute to the understanding of the role played by initial conditions in RD mechanisms, which is a scarcely studied subject in the formation of organized structures like patterns, waves, and oscillatory patterns [46,47].

We found that systems with the same parameters, size, and boundaries can produce different configurations depending on the initial distribution of Fourier modes, and possibly also on the different distributions of random perturbations. Hence, care must be taken when modeling processes involving growth, temporal development, or multiple stages since the stability of solutions in previous steps plays an essential role to define the solution at the next stage. This idea could be fruitful to understand the intraspecific or interspecific variability of phenotypic traits and the role of growth in the formation of biological striped patterns.

Although Eqs. (4)–(9) are not restricted to a particular RD system, our numerical studies on persistency of modes has been applied to the Brusselator system mainly because this model has been extensively used in the field of wavelength

selection [4,7,48–50]. However, as there is experimental and numerical evidence of Eckhaus wavelength selection in the Lengyel-Epstein, Belousov-Zhabotinsky, FitzHugh-Nagumo, and BVAM reaction-diffusion models [51–57], our theoretical analysis is also valid for these systems, but the numerical studies should be done.

In this work, we use the GL approach to study the persistency of patterns. The analysis presented here can be generalized to study the role of nonlinearities and the non-normality of the Laplacian in the pattern transition problem [58].

A possible biological implication is the appealing possibility of using three different elements to control the number of rolls that a pattern solutions can support without losing stability: the domain size, the proximity of the parameters to the bifurcation value and the prepattern. The coupling between multiple steps mechanisms of pattern formation enriches the diversity of spatial information that complex systems form in successive stages, occurring one after other (even at totally different time scales), producing different degrees of variability and robustness to the observable pattern.

ACKNOWLEDGMENTS

Financial support from CONACYT through Grant No. A1-S-8317 is gratefully acknowledged. I.S.-H. acknowledges support by UNAM-DGAPA under Grant No. IN117419.

- [1] P. Arcuri and J. Murray, *J. Math. Biol.* **24**, 141 (1986).
 [2] M. Ipsen, L. Kramer, and P. G. Sørensen, *Phys. Rep.* **337**, 193 (2000).
 [3] P. K. Maini, H. G. Othmer *et al.*, *Mathematical Models for Biological Pattern Formation* (Springer, Berlin, 2001).

- [4] H. Kidachi, *Prog. Theor. Phys.* **63**, 1152 (1980).
 [5] M. C. Cross and P. C. Hohenberg, *Rev. Mod. Phys.* **65**, 851 (1993).
 [6] I. S. Aranson and L. Kramer, *Rev. Mod. Phys.* **74**, 99 (2002).
 [7] B. Peña and C. Pérez-García, *Phys. Rev. E* **64**, 056213 (2001).

- [8] A. De Wit and G. Dewel, *Brisure de Symetrie Spatiale et Dynamique Spatio-Temporelle Dans Les Systemes Reaction-Diffusion* (Université libre de Bruxelles, 1993).
- [9] J. T. Stuart and R. C. DiPrima, *Proc. R. Soc. Lond. A* **362**, 27 (1978).
- [10] W. Eckhaus, *Studies in Nonlinear Stability Theory*, Vol. 6 (Springer Science & Business Media, Berlin, 2012).
- [11] A. Ledesma-Durán and J. L. Aragón, *Chaos, Solitons Fractals* **124**, 68 (2019).
- [12] L. Kramer and H. Riecke, *Z. Phys. B Condens. Matter* **59**, 245 (1985).
- [13] L. Kramer and W. Zimmermann, *Physica D* **16**, 221 (1985).
- [14] H. Shoji, K. Yamada, D. Ueyama, and T. Ohta, *Phys. Rev. E* **75**, 046212 (2007).
- [15] H. Shoji and K. Yamada, *Jpn. J. Ind. Appl. Math.* **24**, 67 (2007).
- [16] L. Kramer, H. Schöber, and W. Zimmermann, *Physica D* **31**, 212 (1988).
- [17] T. Leppänen, M. Karttunen, R. Barrio, and K. Kaski, *Prog. Theor. Phys. Suppl.* **150**, 367 (2003).
- [18] A. J. McKane, T. Biancalani, and T. Rogers, *Bull. Math. Biol.* **76**, 895 (2014).
- [19] A. Sanz-Anchergues, A. M. Zhabotinsky, I. R. Epstein, and A. P. Munuzuri, *Phys. Rev. E* **63**, 056124 (2001).
- [20] E. V. Moran, F. Hartig, and D. M. Bell, *Global Change Biol.* **22**, 137 (2016).
- [21] D. I. Bolnick, P. Amarasekare, M. S. Araújo, R. Bürger, J. M. Levine, M. Novak, V. H. Rudolf, S. J. Schreiber, M. C. Urban, and D. A. Vasseur, *Trends Ecol. Evol.* **26**, 183 (2011).
- [22] A. M. Turing, *Bull. Math. Biol.* **52**, 153 (1990).
- [23] J. Murray, *Mathematical Biology, Vol. II. Spatial Models and Biomedical Applications* (Springer, Berlin, 2003).
- [24] A. Ledesma-Durán, L.-H. Juárez-Valencia, J.-B. Morales-Malacara, and I. Santamaría-Holek, *J. Biol. Phys.* **43**, 247 (2017).
- [25] T. Miura, K. Shiota, G. Morriss-Kay, and P. K. Maini, *J. Theor. Biol.* **240**, 562 (2006).
- [26] R. E. Baker, E. Gaffney, and P. Maini, *Nonlinearity* **21**, R251 (2008).
- [27] E. Crampin, W. Hackborn, and P. Maini, *Bull. Math. Biol.* **64**, 747 (2002).
- [28] A. L. Krause, V. Klika, T. E. Woolley, and E. A. Gaffney, *J. R. Soc., Interface* **17**, 20190621 (2020).
- [29] P. K. Maini and T. E. Woolley, *The Dynamics of Biological Systems* (Springer, Berlin, 2019), pp. 189–204.
- [30] S. Kondo and T. Miura, *Science* **329**, 1616 (2010).
- [31] K. W. Rogers and A. F. Schier, *Annu. Rev. Cell Dev. Biol.* **27**, 377 (2011).
- [32] A. Kicheva, T. Bollenbach, O. Wartlick, F. Jülicher, and M. Gonzalez-Gaitan, *Curr. Opin. Genet. Dev.* **22**, 527 (2012).
- [33] O. Chernova and A. Kiladze, *Biol. Bull. Rev.* **9**, 174 (2019).
- [34] E. G. Moss, *Curr. Biol.* **17**, R425 (2007).
- [35] L. Marcon and J. Sharpe, *Curr. Opin. Genet. Dev.* **22**, 578 (2012).
- [36] J. B. Green and J. Sharpe, *Development* **142**, 1203 (2015).
- [37] D. Dalle Nogare and A. B. Chitnis, *PLoS Biol.* **15**, e2004412 (2017).
- [38] J. D. Glover, K. L. Wells, F. Matthäus, K. J. Painter, W. Ho, J. Riddell, J. A. Johansson, M. J. Ford, C. A. Jahoda, V. Klika *et al.*, *PLoS Biol.* **15**, e2002117 (2017).
- [39] B. Nagorcka, *J. Theor. Biol.* **137**, 127 (1989).
- [40] W. K. Ho, L. Freem, D. Zhao, K. J. Painter, T. E. Woolley, E. A. Gaffney, M. J. McGrew, A. Tzika, M. C. Milinkovitch, P. Schneider *et al.*, *PLoS Biol.* **17**, e3000132 (2019).
- [41] T. Miura, *Sci. Signaling* **6**, pe14 (2013).
- [42] K. Painter, P. Maini, and H. G. Othmer, *Proc. Natl. Acad. Sci. USA* **96**, 5549 (1999).
- [43] A. Nakamasu, G. Takahashi, A. Kanbe, and S. Kondo, *Proc. Natl. Acad. Sci. USA* **106**, 8429 (2009).
- [44] V. Klika, M. Kozák, and E. A. Gaffney, *SIAM J. Appl. Math.* **78**, 2298 (2018).
- [45] R. A. Van Gorder, *Proc. R. Soc. A* **476**, 20200003 (2020).
- [46] A. Ledesma-Durán and J. L. Aragón, *Sci. Rep.* **9**, 11287 (2019).
- [47] A. Ledesma-Durán and J. L. Aragón, *Commun. Nonlinear Sci. Numer. Simul.* **83**, 105145 (2020).
- [48] A. De Wit, D. Lima, G. Dewel, and P. Borckmans, *Phys. Rev. E* **54**, 261 (1996).
- [49] L. Yang, M. Dolnik, A. M. Zhabotinsky, and I. R. Epstein, *J. Chem. Phys.* **117**, 7259 (2002).
- [50] S. P. Kuznetsov, E. Mosekilde, G. Dewel, and P. Borckmans, *J. Chem. Phys.* **106**, 7609 (1997).
- [51] H. Riecke and H.-G. Paap, *Europhys. Lett.* **14**, 433 (1991).
- [52] I. Berenstein, L. Yang, M. Dolnik, A. M. Zhabotinsky, and I. R. Epstein, *Phys. Rev. Lett.* **91**, 058302 (2003).
- [53] S. Rashkeev, M. Glazov, and F. Barlat, *Comput. Mater. Sci.* **21**, 230 (2001).
- [54] M. Bär and L. Brusch, *New J. Phys.* **6**, 5 (2004).
- [55] I. Berenstein and A. P. Muñozuri, *J. Chem. Phys.* **129**, 114508 (2008).
- [56] M. O. Gani and T. Ogawa, *Commun. Nonlinear Sci. Numer. Simul.* **33**, 30 (2016).
- [57] L. Q. Zhou and Q. Ouyang, *Phys. Rev. Lett.* **85**, 1650 (2000).
- [58] V. Klika, *Chaos: Interdiscip. J. Nonlin. Sci.* **27**, 073120 (2017).